



Stability, chemical composition, and structural and electronic properties of the intermetallic compound $\tau_4\text{-(Al}_{1-x}\text{Si}_x)_5\text{Fe}$

C.M. Fang^{*}, Z.P. Que, Z. Fan

Brunel Centre for Advanced Solidification Technology (BCAST), Brunel University London, Uxbridge, Middlesex UB8 3Ph, UK

ARTICLE INFO

Key words:

Fe-containing intermetallic compound
 $\tau_4\text{-Al}_3\text{Si}_2\text{Fe}$ phase
 Si contents
 Crystal structure
 First-principles calculations

ABSTRACT

$\tau_4\text{-(Al}_{1-x}\text{Si}_x)_5\text{Fe}$ particles form during casting of Al-based alloys. They have strong impacts on the solidification process and the mechanical performance of the products. Meanwhile, experiments revealed notable variations in lattice parameters and chemical compositions for the manufactured Al alloys, and knowledge about the intrinsic properties of the τ_4 -phase is still far from complete. We here investigate the crystal chemistry and electronic properties of the τ_4 -phase using a combination of ab initio modelling and thermodynamics analysis. The study justified the $\tau_4\text{-Al}_3\text{Si}_2\text{Fe}$ superstructure at low temperature. There is a shallow potential valley in the formation energy vs Si content curve, corresponding to its compositional and structural flexibility. Thermodynamics analysis revealed kinetic effects on its chemical composition and Al/Si distribution during casting. The obtained information helps understand the formation of and characterize the Fe-IMCs particles in Al alloys, and design novel Al alloys and manufacturing processes for recycling Al.

1. Introduction

Commercial aluminum (Al) metals/alloys contain substantial extents of Fe and Si as constituent alloying elements or impurities [1,2]. The low solubility of Fe in Al (< 0.05 wt%) leads to formation of Al-rich Fe-containing intermetallic compounds (Fe-IMCs) during manufacturing [2,3]. Si is often added into Al alloys for improving the castability and mechanical performance of the alloys [2,4]. Si impurity or addition may stabilize the binary Fe-IMCs, resulting in formation of ternary Al-Fe-Si compounds [1,2,4–6]. The binary Al-Fe and ternary Al-Fe-Si phases constitute an important part of the microstructures of the alloys and determine largely the mechanical performances of the products. Among the Fe-IMCs, the τ_4 -phase has been identified in Al-Si alloys [7–9] and Al-Si-Ni alloys [10,11]. The latter exhibit excellent mechanical performances and have potential applications at high temperatures. The experimental investigations revealed that the newly formed nano-sized τ_4 -phase particles contribute to the improved mechanical performance of the alloys [11]. Meanwhile, sizable Fe-IMCs particles with e.g. plate-like or needle-like morphologies formed during casting deteriorate the mechanical performance of the cast parts [1,4,12]. The deterioration becomes more pronounced for recycling of Al scraps/wastes in which various Fe-IMCs particles have been accumulated during usage, storage and treatments [13–17]. To minimize the

harmful effects of the Fe-IMCs particles, various methods have been applied, including removing the Fe-IMCs particles [12,18] and manipulating casting conditions and/or adding minor elements to transform the harmful Fe-IMCs into less harmful or even beneficial nano-sized particles [10,11,19–21]. To realize such purposes basic information about the crystal chemistry in the related Fe-IMCs phases, including the τ_4 -phase is essential.

The τ_4 -phase [3,22] has other metallurgical nomenclatures including δ - [12,22–25], K4- [22,26] and A-phase [23,27]. The τ_4 -phase forms in Al-based alloys with relatively high Si contents, and the particles display typically a plate-like morphology. In phase characterization the τ_4 -phase is sometime confused with the β -phase since both phases have similar Fe contents and their particles exhibit plate-like morphologies [28,29]. Chemically, the τ_4 -phase has the highest Si content among the Al-rich Al-Fe-Si compounds [1,20,22,28–30]. Crystallographically, there are two structural models used currently for this phase. Pandey and Schubert prepared τ_4 -phase samples by heating an $\text{Fe}_{17}\text{Al}_{50}\text{Si}_{33}$ alloy at 800 °C for 14 h [31]. They determined its crystal structure to be iso-structural with PdGa_5 [32]. It has a tetragonal lattice with space group $I4/mcm$ (no. 140). The lattice parameters were determined to be $a = 6.07 \text{ \AA}$ and $c = 9.50 \text{ \AA}$ [31]. The Al/Si atoms were assumed to be uniformly distributed at the Al Wyckoff sites. Gueneau et al. [30] obtained τ_4 -phase single crystals by heating the $\text{Al}_8\text{Fe}_5\text{Si}_7$ mixture at 1127 °C for 14 h and then

^{*} Corresponding author.

E-mail address: changming.fang@brunel.ac.uk (C.M. Fang).

<https://doi.org/10.1016/j.jalcom.2025.182295>

Received 10 April 2025; Received in revised form 15 July 2025; Accepted 15 July 2025

Available online 16 July 2025

0925-8388/© 2025 The Authors. Published by Elsevier B.V. This is an open access article under the CC BY license (<http://creativecommons.org/licenses/by/4.0/>).

annealing it at 890 °C for another 14 h. Based on the single-crystal X-ray diffraction patterns they refined the crystal structure of the PdGa₅-type with lattice parameters $a = 6.061 \text{ \AA}$ and $c = 9.525 \text{ \AA}$, which is referred to as the average model. The iron atoms occupy the Wyckoff 4a (0,0,1/4) with the local symmetry 422, Al occupy the 4c (0,0,0) with 4/m symmetry and Al/Si mixture at the 16i ($x, x + 1/2, z$) (local symmetry C_2) with $x = 0.15216$, $z = 0.14546$. Meanwhile, they also observed extra diffraction patterns which lead to a superstructure with an orthorhombic lattice with space group Pbcn (no. 60). The same pseudo-tetragonal lattice parameters were used. There are four types of atomic species. Fe occupy the 4c (0,0.0109,1/4) with the local symmetry C_2 , Al1 occupy the 4a (0,0,0) with only inverse symmetry, Al2 at the 8d (0.141, 0.6345, 0.8623) and Si at the 8d (0.1613, 0.6687, 0.1526). The local symmetry of the Al2 and Si atoms is limited to C_1 . Its chemical composition is Al₃Si₂Fe accordingly.

The average model has been widely used by experimentalists for characterizing the τ_4 -phase in Al alloys [12,19–22]. Krendelsberger et al. prepared a series of AlFeSi alloys with various chemical compositions under different thermal treatments. They also determined the crystal structures of the Fe-IMCs in the alloys. The obtained τ_4 -phase was characterized using the average model. Their study revealed variable lattice parameters with $a = 6.0570\text{--}6.1043 \text{ \AA}$ and $c = 9.4954\text{--}9.6542 \text{ \AA}$ for the τ_4 -phase in the alloys [19]. Based on the previous experiments in the literature, Gueneau et al. suggested variable compositions (atomic percentage): Fe 15–17, Si 27–43 and Al 40–48 for the τ_4 -phase. The single crystal they used for the structure determination was measured to have the chemical composition of Al_{2.7}Si_{2.3}Fe deviating from the ideal Al₃Si₂Fe [30]. The extra Si was believed to be distributed at the Al2 (Wyckoff 8d) sites with the structural formula $\tau_4\text{-Al}^I(\text{Al}_{1-x}\text{Si}_x)_2^{\text{II}}\text{Si}_2\text{Fe}$, here the Roman numerals represent the Wyckoff sites for the Al atoms (Fig. 1). Such deviation of the Si content in the samples from the ideal composition means local symmetry breaking in the crystals. The mechanism behind is still unknown. In practice, the difficulties to obtain samples of high purity and the minor difference of diffraction coefficients for Al and Si in the Fe-IMCs limit the accuracy of determination of Al/Si occupations at the Wyckoff sites [12,31,33–35].

Parameters-free first-principles methods have advantages to obtain reliable information about intrinsic properties, such as formation, stability, crystal structure and chemical bonding and electronic structures of the Fe-IMCs [36–39]. Amirkhanyan et al. investigated the mechanical and electronic properties of the τ_4 -Al₃Si₂Fe superstructure [39] using a first-principles approach. Hou et al. [40] studied the structural and electronic properties of several Fe-IMCs including Al₂Si₃Fe by means of the density-functional theory. First-principles calculations were performed for the τ_4 -phase with Fe-Ni alloying [11]. Up to now there is still

a lack of comprehensive understanding about the intrinsic structural properties of the τ_4 -phase. Such understanding is essential to study its potential multicomponent alloys. Herewith we investigate the formation, stability, chemical composition, crystal structure and electronic properties of the τ_4 -phase using an electronic density-functional theory approach. Possible defects in the τ_4 -Al₃Si₂Fe superstructure were studied. Thermodynamics analysis was employed to investigate impacts of the kinetic factors on its stability and chemical composition around the casting temperature. The combined study revealed a shallow potential valley in the curve of the formation energy vs Si content with the superstructure τ_4 -Al₃Si₂Fe being the stable one at low temperature. The configurational entropy contribution stabilizes structures bearing a broad range of Si contents during casting. The information enriches our knowledge about the Fe-IMCs and is useful not only for phase characterization in Al-based alloys, but also for understanding the general chemistry and thermodynamics of the Fe-IMCs, and further for development of new Al-alloys, particularly for circular Al metals [14,15,18,41,42].

2. Methods

During solidification, the iron atoms in the liquid either become solution in solid Al matrix or react with Al (and Si) to form Fe-IMCs. Fe solution in Al bulk (Fe*) together with elemental solids, Al and Si is thus, used as a reference here to address the stability of the τ_4 -phase. The stability of τ_4 -(Al_{1-x}Si_x)₅Fe is assessed by the formation energy,

$$\Delta E_{\text{form}} = E((\text{Al}_{1-x}\text{Si}_x)_5\text{Fe}) - [5(1-x)E(\text{Al}) + 5xE(\text{Si}) + E(\text{Fe}^*)] \quad (1)$$

here, $E((\text{Al}_{1-x}\text{Si}_x)_5\text{Fe})$, $E(\text{Al})$, $E(\text{Si})$ and $E(\text{Fe}^*)$ represent the calculated total valence-electron energies for τ_4 -(Al_{1-x}Si_x)₅Fe, the elemental solids Al and Si, and the effective atom energy of a dilute Fe solution in the Al matrix (Fe*), respectively. The solution energy of a dilute Fe solution in Al, $\Delta E(\text{Fe}^*)$ is defined as,

$$\Delta E(\text{Fe}^*) = E(\text{Al}_n\text{Fe}) - [nE(\text{Al}) + E(\text{Fe})] \quad (2)$$

here, $E(\text{Al}_n\text{Fe})$ and $E(\text{Fe})$ are the calculated total valence-electron energy for Al_nFe and elemental solid Fe, respectively. In this way the effective atom energy of the Fe in the Al matrix is defined as,

$$E(\text{Fe}^*) = E(\text{Al}_n\text{Fe}) - nE(\text{Al}) \quad (3)$$

The term $E(\text{Fe}^*)$ in Eq. (3) is thus obtained for Eq. (1). The unit of $\Delta E(\text{Fe}^*)$ and $E(\text{Fe}^*)$ is eV/Fe. We also performed dilute Si solution in Al using Eq. (2) with Si replacing Fe.

For the dilute solution of Fe or Si in the FCC-Al matrix, a $3a_0 \times 3a_0 \times 3a_0$ supercell (here a_0 is the lattice parameter of α -Al) was used. This

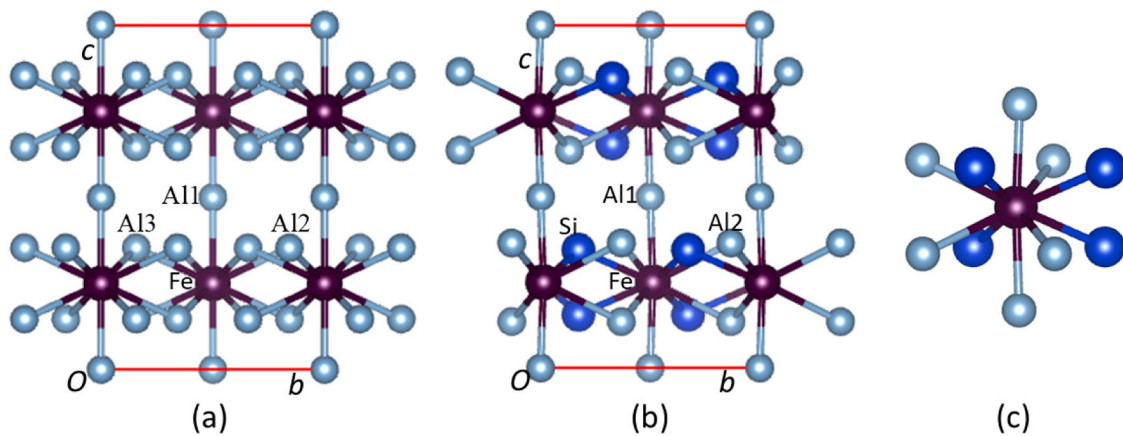


Fig. 1. Schematic structure of novel Al₅Fe (a) and the most stable Al₃Si₂Fe (b). The coordination of Fe in Al₃Si₂Fe is illustrated in (c). The silvery-grey spheres represent Al, the blue Si and the dark-brown Fe. The atomic species is illustrated in Figs. 1a and 1b. For simplicity bonds longer than 2.6 Å are not linked in Figs. 1a and 1b.

supercell contains 107 Al atoms and one impurity atom. A $2a_0 \times 2b_0 \times c_0$ supercell (here a_0 , b_0 , c_0 are the lattice parameters of the conventional unit cell [30]) was utilized for investigating the intrinsic defects and Si doping in τ_4 -Al₃Si₂Fe and novel τ_4 -Al₅Fe.

The first-principles code Vienna Ab initio Simulation Package (VASP) [43,44] was employed in this study. This code utilizes a pseudopotential plane-wave scheme within the density functional theory [45]. It exerts the projector augmented wave method [46] and the exchange and correlation terms are handled by means of the spin-polarized generalized gradient approximation (GGA) with the scalar relativistic approximation [47]. The previous studies revealed that the GGAs work better than the local density approximation for the compounds containing 3d transition metals, e.g. Fe [5,11,48].

The cut-off energy was 400.0 eV for the wave functions and 550.0 eV for the augmentation functions, respectively. The employed energies are higher than the default values, $E_{\text{NMAX}}/E_{\text{AUG}} = 245.3 \text{ eV}/322.1 \text{ eV}$ for Si, 240.4 eV/291.1 eV for Al and 267.9 eV/511.9 eV for Fe, respectively. Such high cut-off energies provide results of high accuracy and reliability. The NPT ensemble was adopted. The energy and force convergence criteria are 10^{-4} eV and 10^{-3} \AA/eV , respectively, when finding an equilibrium structure. Dense k -meshes were employed, e.g. $12 \times 12 \times 8$ ($84\text{--}576 \text{ } k$ -points) and $6 \times 6 \times 8$ ($24\text{--}144 \text{ } k$ -points) for the Brillouin zones of the conventional cell and the $2a_0 \times 2b_0 \times c_0$ supercell, respectively using the Monkhorst-Pack approach [49]. Tests of the cut-off energies and k -meshes displayed good convergences of the calculations with energy deviations being less than 1 meV/atom.

3. Results and discussions

3.1. The novel τ_4 -Al₅Fe and the superstructure τ_4 -Al₃Si₂Fe

First-principles calculations were first performed for the elemental solids, Al, Si and Fe and the dilute solutions of Fe and Si in Al matrix, as well as the novel binary τ_4 -Al₅Fe and the ternary superstructure τ_4 -Al₃Si₂Fe [30]. The results are presented in Supplementary materials, Table S-1. The crystal structures for the novel binary τ_4 -Al₅Fe, the superstructure τ_4 -Al₃Si₂Fe and the coordination of Fe in the latter were shown in Fig. 1a–c, respectively.

The calculated lattice parameters for the elemental solids, Al, Fe and Si are in good agreements with the experimental values extended to 0 K [50] with deviations within 1 % (Table S-1). The calculations produced the ferromagnetic solution for α -Fe with a local moment of 2.18 μ_B which is close to the experimental value [51]. This moderate value of the magnetic moment corresponds to the weak ferromagnet nature of α -Fe [51].

A dilute Fe solution in Al becomes non-magnetic with a solution energy of -0.46 eV/Fe . Meanwhile, a dilute Si solution in Al costs an energy as high as 0.43 eV/Si, agreeing with the previous calculations [5, 38]. This indicates that Si solution in Al at ambient conditions is unlikely. Therefore, we use bulk Si as reference in Eq. (1).

The calculations for novel τ_4 -Al₅Fe provided a non-magnetic solution with a formation energy -0.64 eV per formula unit/or per Fe (Table S-1), indicating its stability with respect to the elemental Al and Fe solution in Al. However, this value is notably higher than that of θ -Al₁₃Fe₄ (-1.13 eV/Fe) using the same method [5,52,53], indicating that the binary τ_4 -Al₅Fe is less competent to form as a primary phase in Al alloys during casting. The calculated lattice parameters of this novel binary compound are also notably larger than that of the ternary compound [30].

The formation energy for the superstructure τ_4 -Al₃Si₂Fe is -1.08 eV/Fe with a non-magnetic solution. This value is notably lower than that of the novel τ_4 -Al₅Fe. This reflects the strong Si stabilization effect. Moreover, this formation energy is even lower than of the θ -Al₁₃Fe₄ [5,54]. This indicated that τ_4 -Al₃Si₂Fe particles may form as a primary phase during casting, in agreement with the experimental observations [9]. The calculations also revealed that the τ_4 -Al₃Si₂Fe

superstructure exhibits an orthorhombic lattice with the lattice parameters close to the pseudo-tetragonal cell from the previous density-functional theory calculations [39] and the experimental values [30,31].

The calculated atomic coordinates and local chemical bonding for τ_4 -Al₃Si₂Fe are listed in Table S-2 with the experimental data [30] for comparison. The calculated fractional coordinates of atoms in the τ_4 -Al₃Si₂Fe superstructure clearly agree with the experimental measurements [30] within deviations less than 0.01.

Each Si has two Fe, six Al and one Si neighbours (Figs. 1b and 1c). There is a long Si-Al2 with a length of 3.12 \AA . Each Al1 has two Fe, four Al and four Si neighbours, meanwhile, an Al2 atom has two Fe, three Al and four Si and one long Al2-Si bond.

We also performed calculations the configuration for τ_4 -Al₃Si₂Fe with the Si full occupation at the Al2 sites and Al occupying the original Si sites which correspond to the Al3 sites in the novel τ_4 -Al₅Fe phase (Fig. 1). The calculations produced similar lattice parameters and formation energy as the one reported. This agrees with the fact that both Al2 and Si(Al3) sites have the same local symmetry.

3.2. Intrinsic defects in τ_4 -Al₃Si₂Fe superstructure and novel τ_4 -Al₅Fe

Intrinsic defects may form in the Fe-IMCs during manufacturing at elevated temperatures (around 700 °C) [5,52,53]. They have impacts on the formation, stability and properties of the compounds. Several possible intrinsic defects including vacancies, replacing Al by Fe, Fe by Al, Fe by Si and Si by Fe in the novel τ_4 -Al₅Fe and the ternary τ_4 -Al₃Si₂Fe superstructure were investigated. Configurations for different Si occupations in τ_4 -Al₃Si₂Fe were included in the study. The calculated results for the latter are listed in Table 1. The results for the former defects are listed in Table 2. The chemical bonding in the configurations were analyzed with the numbers of Si-Si bonds in each configuration were included in Table 1.

As shown in Table 1, moderate energy costs for one exchange of Si at the Si site and Al at the Al1 (0.10 eV, conf.3) and the Al2 sites (0.07 eV, conf.2). Structural analysis revealed that the Si/Al exchanges increase the number of Si-Si pairs from four in the ideal configuration to six per unit cell. This result indicates repulsive nature of the Si-Si bonds formed in the Fe-IMCs. Meanwhile, exchanging more Si/Al atoms (Conf.4 and

Table 1

Energy costs for different Si occupation site in τ_4 -Al₃Si₂Fe. The energy cost with respect to the most stable configuration is $\Delta E = E(\text{conf.}) - E(\tau_4\text{-Al}_3\text{Si}_2\text{Fe})$. We include the symmetry, calculated (averaged) lattice parameters and number of Si-Si bonds in the configurations. Here Si1, Si2 and Si3 represent Si atoms at the Al1, Al2 and Si sites in [30].

Configuration	Space group	Latt.e paras. (\AA)	ΔE (eV/cell)	N(Si-Si) per cell
Conf.1: (ideal [30])	Orth. <i>Pbcn</i> (Nr. 60)	$a = 6.057$ $b = 6.061$ $c = 9.483$ $V = 348.17 \text{ \AA}^3$	0.00	four Si-Si bonds.
Conf.2: 7Si3 + 1Si2	Triclinic <i>P1</i> (nr. 1)	$a = 6.092^*$ $b = 6.088$ $c = 9.399$ $V = 348.59 \text{ \AA}^3$	+ 0.07	six Si-Si bonds
Conf.3: 7Si3 + 1Si1	Triclinic <i>P1</i> (nr. 1)	$a = 6.062^*$ $b = 6.066$ $c = 9.515$ $V = 349.89 \text{ \AA}^3$	+ 0.10	six Si-Si bonds
Conf.4: 4Si2 + 4Si3	Triclinic <i>P1</i> (nr. 1)	$a = 6.052^*$ $b = 6.036$ $c = 9.671$ $V = 353.26 \text{ \AA}^3$	+ 0.27	eight Si-Si bonds
Conf.5: 4Si3 + 4 Si1	Triclinic <i>P1</i> (nr. 1)	$a = 6.175^*$ $b = 6.169$ $c = 9.204$ $V = 350.55 \text{ \AA}^3$	+ 0.55	nine Si-Si bonds

Table 2

Calculated formation energies for intrinsic defects (Al/Fe vacancies, Fe at Al/Al2 sites, Si at Al1/Al2 sites, Fe replaced by Al, Fe replaced by Si) in the novel τ_4 -Al₅Fe and the superstructure τ_4 -Al₃Si₂Fe based the methods in [52]. The Si sites at τ_4 -Al₃Si₂Fe superstructure corresponds to the Al3 sites in the novel τ_4 -Al₅Fe. The energy costs for the intrinsic defects refer to the τ_4 -Al₃Si₂Fe superstructure, the elemental solids Al and Si and solute Fe in Al matrix [52].

Defect type	τ_4 -Al ₅ Fe	τ_4 -Al ₃ Si ₂ Fe
Al1 vacancy	+ 1.97	+ 1.12
Al2 vacancy	+ 1.06	+ 1.21
Si/Al3 vacancy	+ 1.06	+ 1.45
Fe vacancy	+ 1.32	+ 2.60
Al1 by Fe	+ 0.60	+ 0.94
Al2 by Fe	+ 1.20	+ 1.08
Si/Al3 by Fe	+ 1.20	+ 1.87
Al1 by Si	- 0.17	+ 0.23
Al2 by Si	- 0.18	+ 0.18
Fe by Al	+ 0.91	+ 2.60
Fe by Si	-	+ 3.12

Conf_5 in Table 2a) causes higher numbers of Si-Si pairs. Consequently, the structure becomes notably less stable. The moderate energy costs for Si/Al exchanges (Conf_2 and Conf_3) suggest that the Si distributions differ from the ideal superstructure model [30] at elevated temperatures at which conditions kinetic factor plays a role. Moreover, the calculated lattice parameters for conf_2 and conf_3 in Table 1 differ moderately from those of the superstructure (Conf_1). The energy-cost difference for the different configurations also means energy-hierarchy in this phase.

Table 2 lists the formation energy costs for various defects in the novel τ_4 -Al₅Fe and the superstructure τ_4 -Al₃Si₂Fe structures. Formation of any vacancy at the Al, Fe and Si sites costs energies over 1 eV in both compounds. Replacing an Fe atom by Al or Si, and Si by Fe costs high energies ranging from 0.9 eV to 3.1 eV. Energy costs to replace one Al2 or Al3 atom by Fe are above 1 eV. Replacement of an Al1 atom by Fe which costs 0.6 eV. These high energy costs mean highly unlikely for formation of these defects even at the casting temperature.

Adding an extra Si in the Al sites in the superstructure τ_4 -Al₃Si₂Fe costs moderately (~0.2 eV). Analysis revealed that one extra Si at the Al sites enhances the number of Si-Si pairs in the cell. Meanwhile, replacing Al by Si in the novel τ_4 -Al₅Fe structure gains energies. The former corresponds to the stability of the superstructure [30] and the latter means favor of Si solutions at the Al sites in the novel binary crystal.

3.3. Si solution at the Al sites in τ_4 -(Al_{1-x}Si_x)₅Fe

Present calculations revealed that Si solution at the Al sites in the novel τ_4 -Al₅Fe enhances its stability, meanwhile extra Si solution in the superstructure τ_4 -Al₃Si₂Fe costs moderate amounts of energy. Moreover, the experiments showed variable Si contents in the τ_4 -phase samples [19,30]. Therefore, it is necessary to study the relation between stability of the τ_4 -phase and the Si content in a systematic way.

Based on the superstructure [30], various configuration of Si solutions in the Al/Si sites in τ_4 -(Al_{1-x}Si_x)₅Fe were studied. The relation between formation energy and Si content for the highly stable configurations is shown in Fig. 2. Fig. 3 shows the relations between the lattice parameters/volume and Si contents in the highly stable τ_4 -phase.

Fig. 2 showed that in τ_4 -Al₅Fe, increasing Si content at both Al1 or Al3 sites lowers down the formation energies. The formation energy reaches a minimum with $x = 0.2$ which the Si occupy fully the Al1 sites. Addition of extra Si atoms at the other Al2 or Al3 sites causes formation of extra Si-Si bonds. Correspondingly the formation energy increases strongly (the red spheres in Fig. 2).

The energy minimum is reached with Si fully occupying the Al3 sites, forming the compositions of τ_4 -Al₃Si₂Fe, the ideal superstructure [30]. Further addition of Si atoms increases the formation energy. This relates to increasing number of Si-Si bonds. For example, in the crystal with chemical formula (Al_{0.55}Si_{0.45})₅Fe, the number of Si-Si bonds is eight

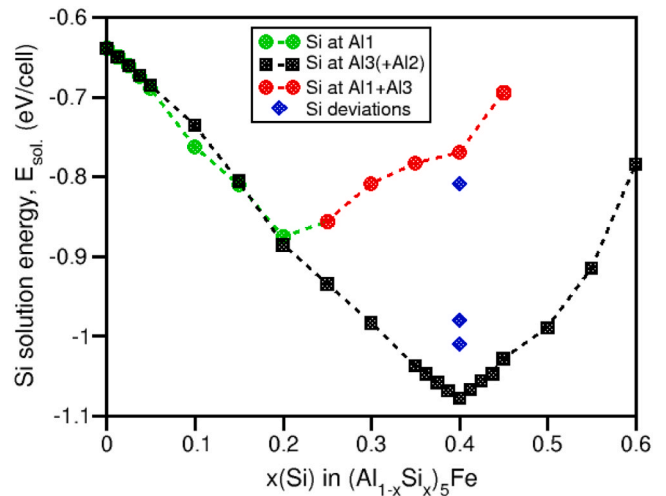


Fig. 2. Calculated formation energies for the stable configurations of the (Al_{1-x}Si_x)₅Fe ($x = 0.0$ – 0.60) with respect to the elemental solids Al, Si and Fe solution in Al matrix according to Eq. (2). The formation energies for configurations with Si at different sites deviating from the τ_4 -Al^IAl^{II}Si^{III}Fe are included (blue diamonds). The dotted lines are used to guide readers' eyes.

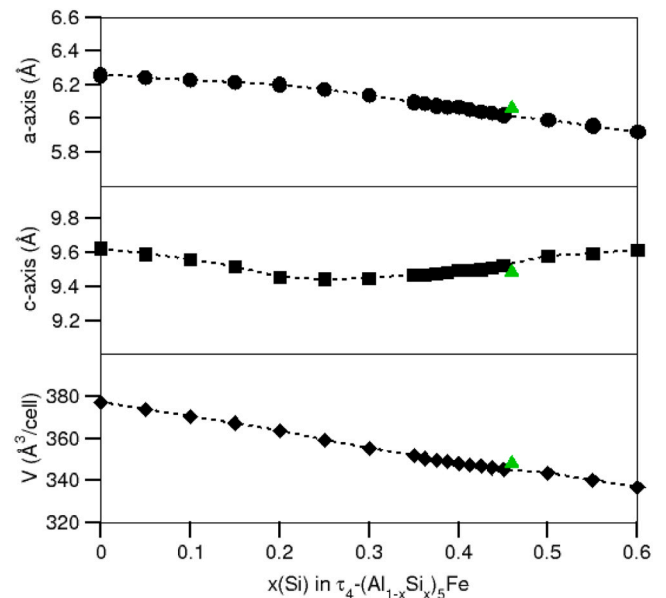


Fig. 3. The calculated relations between the a -axis (top), c -axis (middle) and volume of the conventional cell of τ_4 -(Al_{1-x}Si_x)₅Fe (bottom) and the Si contents. The general structural formula is τ_4 -Al^IAl^{II}(Al_{1-x}Si_x)₂^{III}Fe for $x < 0.40$ and τ_4 -Al^I(Al_{1-x}Si_x)₂^{II}Si^{III}Fe for $x > 0.40$, here the Roman numerals in superscript represent the Al sites. The experimental values (filled green triangles) [30] are included for comparison.

with the extra Si at one of the Al1 or Al2 sites and thus, the stability of the structure is reduced.

As shown in Fig. 3 (bottom), there is an almost linear relation between the cell volume and the Si content. With increasing Si content, the length of a -axis decreases moderately at first (from $x(\text{Si}) = 0.0$ – 0.20) and then it decreases faster. The behavior of c -axis is more complex. With increasing Si content up to 0.25, the length of the c -axis decreases and it then increases moderately with Si content.

The experimental lattice parameters from the single-crystal structure determination for τ_4 -Al_{2.7}Si_{2.3}Fe [30] were included into Fig. 3 for comparison. Clearly, the experimental data are close to the predicted values.

3.4. Chemical bonding and electronic properties of τ_4 -phase

Electronic structure calculations were performed for the τ_4 -Al₃Si₂Fe superstructure. The iso-surfaces of the electron density distributions with $\rho_0(r) = 0.045e/\text{\AA}^3$ is displayed in Fig. 4i and the density of states for selected atoms were plotted in Fig. 4ii, respectively. Fig. 5a showed the dispersion curves along the high-symmetry lines of the Brillouin zone (Fig. 5b).

The curve of the total density of states curve (Fig. 4ii_e) displays one broad band, starting from -12.14 eV. Analysis revealed that the bottom of the band is at Γ , (0,0,0) of the Brillouin zone (Fig. 5b) and it consists of Si 3s mixing with some Al 3s and Fe 4s characters from the eigen character analysis. The total density of the states of the valence band (from the bottom to the Fermi level) increases with increasing energy from the bottom to about -2 eV. There are several peaks at the energy ranging from -2.0 eV to -0.6 eV. Fig. 4ii_e shows a broad valley from -0.5 eV to $+1.0$ eV with a deep well (pseudo gap) at about $+0.59$ eV.

Fig. 4ii shows that the Al/Si 3s and 3p states mix all over the whole valence and conduction bands. The Si/Al 3s states dominate the lower part of the valence band from the bottom to about -6.0 eV. From about -4.0 eV the Si/Al 3p states have higher densities than the 3s states. The Fe 3d states dominate the curve around the Fermi level (-4.0 to 3.0 eV).

Fig. 4i shows high electron density around the Si-Fe bonds, which seems like a two-dimensional (2D) nature for this compound. We performed eigen characters for the three states at Γ around the Fermi level. The state at -0.28 eV at Γ is composed mainly of Fe 3d_{xy} and some Fe 3d_{yz} components. The state at 0.23 eV above the Fermi level consists dominantly of Fe 3d_{xy}² components and the state at $+0.38$ eV Fe 3d_{yz} components. These results indicate three-dimensional (3D) character of this crystal. The 3D character is justified by the dispersion curves crossing the Fermi level along A- Γ and Y-M lines (Fig. 5a).

To obtain more direct knowledge about the interatomic interaction in τ_4 -Al₃Si₂Fe crystal, Bader charge analysis [55,56] was employed. This method was implanted by Henkelman et al. into VASP [57]. The analysis provided charges at the atomic species: $+0.8e/\text{Al}$ at Al1, $+0.6e/\text{Al}$ at Al2, $-1.1e/\text{Si}$ and $-0.5e/\text{Fe}$. The charges at the atomic sites correspond well to the Pauling electronegativity values: 1.61 for Al, 1.90 for Si and 1.83 for Fe in Pauling unit [58]. The highly ionic nature of Si atom in this ternary phase is responsible for the repulsive Si-Si interaction which formation reduces the stability of the crystal.

In the periodic table of elements, Al and Si are neighbours with the latter having one more electron. Therefore, Si solution at the Al sites

means increasing of the number of electrons in the crystal. We calculated the electronic structures for τ_4 -(Al_{0.55}Si_{0.45})₅Fe which is close to the chemical composition in the prepared crystal (Al_{2.7}Si_{2.3}Fe) [30]. The calculated dispersion curves along the high symmetry lines in the Brillouin zone (Fig. 5b) are displayed in Fig. 6i and the related partial density of states for the two different Fe atoms in and total density of states of the compound are shown in Fig. 6ii.

Overall, both the dispersion curves and density of states curves of τ_4 -(Al_{0.55}Si_{0.45})₅Fe (Fig. 6) display strong similarities to the corresponding ones for τ_4 -Al₃Si₂Fe (Fig. 5a and 4ii), respectively. This indicates availability of the rigid band filling model. However, a careful look provided some subtle differences.

- 1) For τ_4 -(Al_{0.55}Si_{0.45})₅Fe, the lowest state is at -12.44 eV which is 0.3 eV lower than that of τ_4 -Al₃Si₂Fe.
- 2) There are rather flat dispersion curves from Y to R above the Fermi level in Fig. 6i, which corresponds to the small peak at 6ii_c at about 0.17 eV for τ_4 -(Al_{0.55}Si_{0.45})₅Fe. This peak about 0.2 eV lower than that for τ_4 -Al₃Si₂Fe (Figs. 4ii and 5a). Moreover, the position of the valley in the curves of the total density of states of τ_4 -(Al_{0.55}Si_{0.45})₅Fe (Fig. 6ii_c) is at $+0.44$ eV which is 0.15 eV lower than that of τ_4 -Al₃Si₂Fe (0.59 eV) as shown in Fig. 5ii_e.
- 3) The Fermi level in the tDOS curve of τ_4 -Al₃Si₂Fe is at a small peak which has density of 2.0 states/eV, meanwhile the Fermi level in the tDOS curve of τ_4 -Al_{2.75}Si_{2.25}Fe is at a small valley with density of 1.5 states/eV, lower than that of τ_4 -Al₃Si₂Fe.

The above results mean a shift of the tDOS curve in τ_4 -(Al_{0.55}Si_{0.45})₅Fe as compared with that of τ_4 -Al₃Si₂Fe and availability of the rigid band filling model for τ_4 -phase. τ_4 -(Al_{0.55}Si_{0.45})₅Fe has a lower density of states at the Fermi level, indicating high stability of the system according to Stoner [59]. Meanwhile, the formation energy increases significantly as shown in Fig. 2 due to the increased number of Si-Si bonds: there are seven Si-Si pairs for τ_4 -(Al_{0.55}Si_{0.45})₅Fe, three more than that in τ_4 -Al₃Si₂Fe (Tables 2 and 3a). Further increment of Si may lead to a more stable compound. This might be the origin of formation of a more stable phase, Al₂Si₃Fe which is a semiconductor [40]. The relation between electron counting and phase stability works for various intermetallic compounds [20,27,60–62].

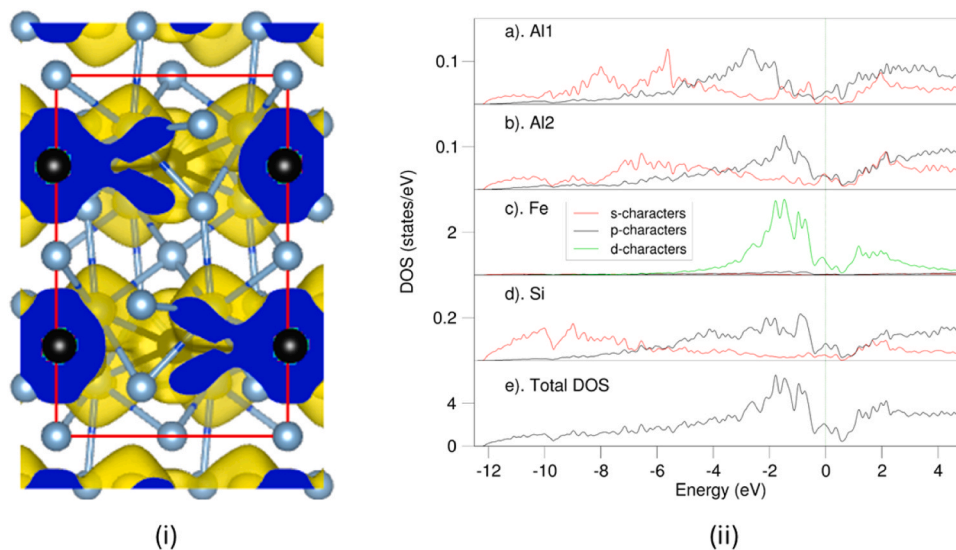


Fig. 4. (i) Iso-surfaces of electron density distribution ($\rho_0(r) = 0.045e/\text{\AA}^3$) and (ii) partial density of states for the atom species (a–d) and total density of states for the superstructure τ_4 -Al₃Si₂Fe [30]. The perpendicular dark-green dotted lines represent the Fermi level (at 0 eV) in (ii).

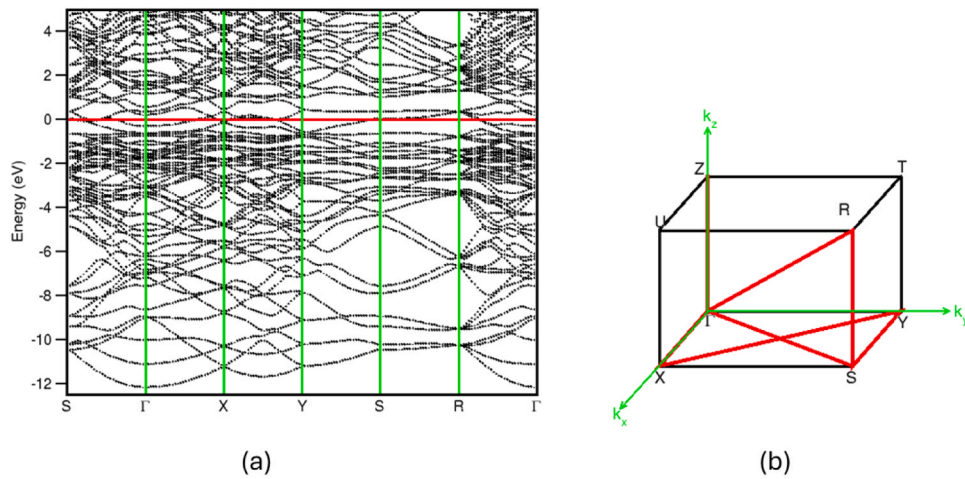


Fig. 5. (a) Dispersion curves along the high-symmetry lines in (b) the Brillouin zone of an orthorhombic lattice of τ_4 - $\text{Al}_3\text{Si}_2\text{Fe}$. The horizontal red line at 0 eV in (a) represents the Fermi level.

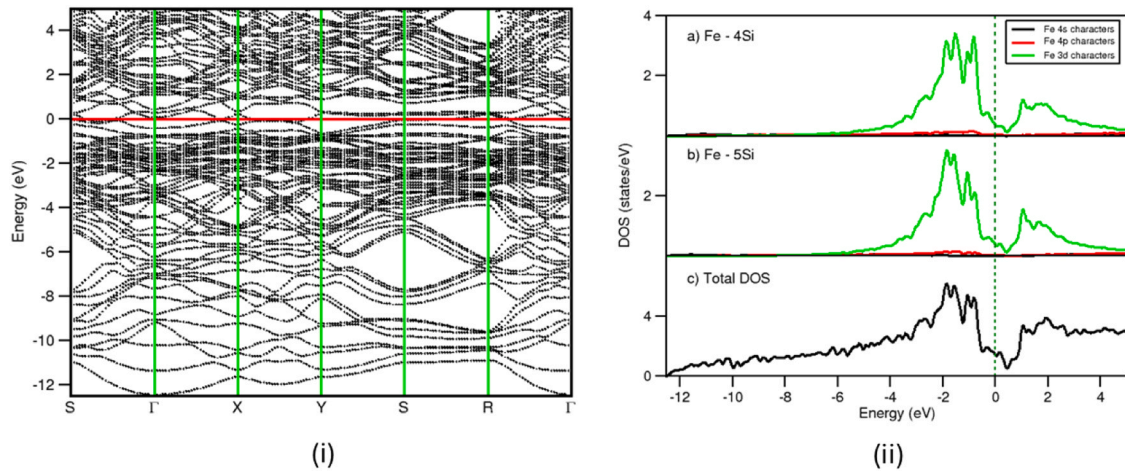


Fig. 6. (i) Dispersion curves along the high-symmetry lines in the Brillouin zone of a pseudo-orthorhombic lattice (Fig. 5b) for τ_4 - $(\text{Al}_{0.55}\text{Si}_{0.45})_5\text{Fe}$. The horizontal red line in (i) and the perpendicular dotted dark green lines in (ii) at 0 eV represent the Fermi level.

4. Thermodynamics analysis on Si content in τ_4 - $(\text{Al}_{1-x}\text{Si}_x)_5\text{Fe}$ during casting

The stability of the τ_4 - $\text{Al}_3\text{Si}_2\text{Fe}$ superstructure was further investigated via exchanging a Si atom and an Al atom at the Al1 or Al2 sites in the $2a_0 \times 2b_0 \times 1c_0$ supercell (a_0, b_0, c_0 are the lattice parameters of the conventional cell). The calculations confirmed the previous calculations with energy cost of 0.39 eV for exchanging one Si with an Al1 atom and 0.27 eV for Al2 in this supercell, which correspond to the values in the conventional cell (Table 1). This result means i) there is a moderate energy hierarchy for Si at the Al sites and ii) there are extra configurations caused by both Al occupation at the Si sites and the Si occupation at the Al sites. The latter indicates configurational entropy contributions in the system at elevated temperatures. Here we analyze the relation between the energy hierarchy of the Si/Al exchange and configurational entropy contributions to the stability.

The change of the free energy of the system at temperature T depends on the formation enthalpy (ΔH) and configurational entropy contributions according to the Gibbs relation:

$$\Delta G = \Delta H - T \Delta S \quad (4)$$

here T is the temperature and $\Delta S = R \ln w$, and $R (= 8.6173 \times 10^{-5} \text{ eV/K})$ is the Boltzmann constant and w represents the number of

configurations. Two possible models are employed here. Model I relates to the Si occupying randomly all the Al and Si sites, and Model II the Si occupying only the Al2/Si sites in the superstructure model.

For the supercell of τ_4 - $\text{Al}_3\text{Si}_2\text{Fe}$ structure, if one Si-Al exchange occurs, there are ($w_1 =$) 32 configurations at the Si sites, and ($w_2 =$) 48 at the Al sites (Al1 + Al2). Thus, the total number of configurations, $w = w_1 \times w_2$ for Model I. For model II, $w_1 = 32$ and $w_2 = 32$. Then, for one Al-Si exchange we obtain $\Delta S = 6.32 \times 10^{-4} \text{ eV/K}$ for Model I and $\Delta S = 5.97 \times 10^{-4} \text{ eV/K}$ for Model II according to Eq. (4).

For $\Delta G = \Delta H - T_c \Delta S = 0$, the critical temperature $T_c = \Delta H/\Delta S$. Then, we obtain $T_c = 430 \text{ K}$ for $\Delta H = 0.27 \text{ eV}$ for Si at Al2 and $T_c = 620 \text{ K}$ for $\Delta H = 0.39 \text{ eV}$ for Si at Al1 for Model I. For Model II, $T_c = 450 \text{ K}$ for $\Delta H = 0.27 \text{ eV}$ for Si at Al2 and $T_c = 660 \text{ K}$ for $\Delta H = 0.39 \text{ eV}$ for Si at Al1. For both models, if temperature is higher than 660 K, the Si atom can occupy both Al1 and Al2 sites.

The above discussion provided a potential evolution path of τ_4 - $\text{Al}_3\text{Si}_2\text{Fe}$ with Si distribution on temperature: τ_4 - $(\text{Al}_{0.6}\text{Si}_{0.4})_5\text{Fe}$ (Model I) transforms to τ_4 - $\text{Al}^{\text{I}}(\text{Al}_{0.6}\text{Si}_{0.4})_4^{\text{II+III}}\text{Fe}$ (model II) at 620 K to ordered τ_4 - $\text{Al}_3\text{Si}_2\text{Fe}$ superstructure at 430 K.

The temperatures for preparing τ_4 - $\text{Al}_3\text{Si}_2\text{Fe}$ samples are 1073 K [31] or 1163 K [30]. The experimental observations revealed formation of this phase during casting ($\sim 930 \text{ K}$) [11]. These temperatures are notably higher than the critical temperature (660 K). Thus, we can

Table 3

The chemical composition and lattice parameters of τ_4 -phase from the present calculations and the experimental data from the available literature [8,27,30,31,39] and the new experiment for Al-13.0Si-3.0Fe alloy [63]. *The lengths of the in-plane axis are the averaged since those of *a*- and *b*-axis differ moderately (< 1 %).

Authors/year	Details of ally and method	τ_4 -composition	Latt.paras. (Å)
This work	DFT-GGA	1). Al ₃ Si ₂ Fe (superstructure) [30] 2). (Al _{0.55} Si _{0.45}) ₅ Fe 3). (Al _{0.50} Si _{0.50}) ₅ Fe	<i>a</i> = 6.059*, <i>c</i> = 9.496 <i>a</i> = 6.020*, <i>c</i> = 9.524 <i>a</i> = 5.989*, <i>c</i> = 9.578
Amirkhanyan (2014) [39]	DFT-GGA	Al ₃ Si ₂ Fe superstructure [30]	-
Pandy (1969) [31]	an Fe ₁₇ Al ₅₀ Si ₃₃ alloy Heat at 800 °C for 14 h XRD powder diffraction	- average model [30,31]	<i>a</i> = 6.07, <i>c</i> = 9.50
Gueneau (1995) [30]	An Al ₈ Fe ₅ Si ₇ mixture heat at 1127 °C for 14 h, then annealed at 890 °C for another 14 h. Single crystal determination.	i) (Al _{0.54} Si _{0.46}) ₅ Fe (average model) ii). Al _{2.7} Si _{2.3} Fe mixed model [30]	<i>a</i> = 6.061, <i>c</i> = 525 <i>a</i> = 6.061, <i>c</i> = 525
Krendelsberger (2007) [27]	1). Al ₄₀ Si ₃₈ Fe ₂₂ alloy 2). Al ₄₂ Si ₄₀ Fe ₁₈ alloy 3). Al ₅₀ Si ₂₉ Fe ₂₁ alloy 4). Al ₅₃ Si ₃₃ Fe ₁₄ alloy 5). Al ₆₀ Si ₂₀ Fe ₂₀ alloy The alloys were heated at 550 °C for 1 month. XDR diffraction	- - - - - Average model [30,31]	<i>a</i> = 6.062, <i>c</i> = 9.520 <i>a</i> = 6.057, <i>c</i> = 9.542 <i>a</i> = 6.056, <i>c</i> = 9.552 <i>a</i> = 6.104, <i>c</i> = 9.454 <i>a</i> = 6.101, <i>c</i> = 9.503 <i>a</i> = 6.054, <i>c</i> = 9.497
Que (2025) [63]	Al-13.0Si-3.0Fe alloy Liquid poured out at 720 °C HR-TEM	- Average model [30,31]	<i>a</i> = 6.054, <i>c</i> = 9.497
Li (2000) [8]	Al-Fe-Si at 600 °C	(Al _{1-x} Si _x) ₅ Fe <i>x</i> ≈ 0.33–0.45	-

conclude that at the formation temperatures, the τ_4 -phase samples have their Si distributed at both the Al1 and Al2 and Si sites (Model I). In the other word, the average model works [30,31] for experiments, considering the low diffusion processes at temperatures below 660 K in the Al-based alloys.

The above discussion also suggests availability of a random Al/Si distribution for assessing the stability of this phase on Si contents [30,31]. Two models are chosen: Model I (Si at Al1, Al2 and Al3(Si) sites); and Model II with Si at the Al2 and Al3(Si) sites, based on the calculated results (Fig. 2). We choose *T* = 1000 K to illustrate the temperature effects on the stability of the τ_4 -phase with Si contents. The obtained results are shown in Fig. 7.

The present analysis provides us the following results.

- 1) Fig. 2 showed a shallow potential well at 0 K for the ground state τ_4 -(Al_{1-x}Si_x)₅Fe phase with moderate dependences of formation energy on Si content: *x*(Si) = 0.35, ΔE = 0.04 eV/cell or 1.7 meV/atom; *x*(Si) = 0.45, ΔE = 0.05 eV/cell or 2.0 meV/atom with respect to the most stable τ_4 -Al₃Si₂Fe superstructure.
- 2) For Model II with Si at the Al2 and Al3(Si) sites, the maximum configurational entropy contribution is for *x*(Si) = 0.40. Thus, the local potential well becomes deeper: *x*(Si) = 0.35, ΔG = 0.05 eV/cell or 2.0 meV/atom and *x*(Si) = 0.45, ΔG = 0.06 eV/cell or 2.5 meV/atom with respect to the τ_4 -Al₃Si₂Fe superstructure.
- 3) For Model I with Si at all the Al/Si sites, the maximum contribution of configurational entropy is for *x*(Si) = 0.50. Thus, the Si-rich is favored: *x*(Si) = 0.35, ΔG = 0.08 eV/cell or 3.5 meV/atom,

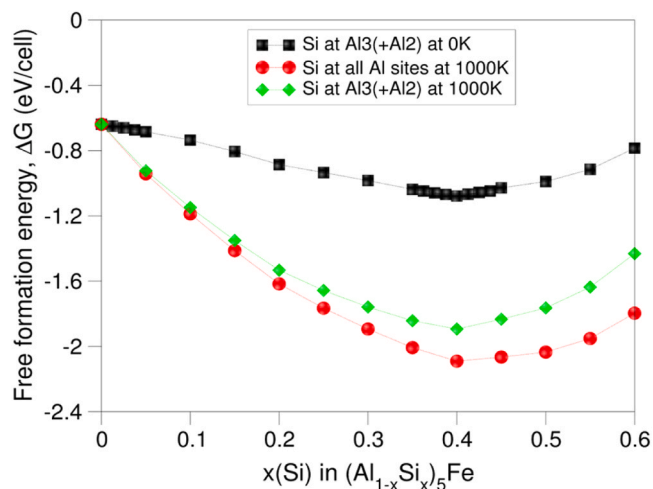


Fig. 7. Thermodynamics analysis for the configurational entropy contributions to the free formation energy of Si content in τ_4 -(Al_{1-x}Si_x)₅Fe (*x* = 0–0.6) crystals at 1000 K with the two random models. The formation energies at 0 K are included for comparison. The dotted lines linking the points are used to guide readers' eyes.

meanwhile, *x*(Si) = 0.45, ΔG = 0.025 eV/cell or 1.0 meV/atom, for *x*(Si) = 0.55, ΔG = 0.06 eV/cell or 2.3 meV/atom with respect to τ_4 -Al₃Si₂Fe.

Since the preparation temperatures are notably higher than the critical point for the Si random occupation at all the Al sites (Model I) in the τ_4 -particle, the chemical formula is better described as, τ_4 -(Al_{1-x}Si_x)₅Fe (the average model [30]). Moreover, at the preparation temperature, the fraction of the substitution Si atoms can be higher than that of the ideal composition, depending on local chemical and thermodynamical conditions.

When temperature lowers down, the contribution of thermodynamics factors including configurational entropy decreases according to Eq. (4). At the same time the Si content and distribution in the crystals change towards more ordered with composition approaching to the ideal superstructure [30] when the samples kept at a low temperature for a reasonably long period.

The present first-principles calculations and thermodynamics analysis revealed compositional and structural flexibility of the τ_4 -phase. They also provide an opportunity to revisit the experiments in the literature [27,30,31]. The ternary Al-Fe-Si diagrams at high temperatures showed a very narrow range for Fe content in the τ_4 -phase [8,22,23]. The Si content varies notably in the experimental observations [27,30,63] and the phase diagrams at elevated temperatures [8,22,23]. For example, the section of the Al-Fe-Si ternary phase diagrams at 600 °C provided a broad range of Si content with *x* = 0.33–0.45 in the formula (Al_{1-x}Si_x)₅Fe (Table 3), which is in line of our study (Fig. 7). Moreover, we also performed structural analysis on τ_4 -phase particles formed in an Al-13.0Si-3.0Fe alloy which was cast at 720 °C [63]. Table 3 lists the calculated lattice parameters for τ_4 -(Al_{1-x}Si_x)₅Fe with *x* = 0.40, 0.45 and 0.50 and the available experimental data in the literature, where the composition of the Al-alloy and preparation conditions are included.

Although there are many publications revealed the formation of the τ_4 -phase particles in high-Si Al alloys, most of them are about phase characterization and structural determination but contain no compositional analysis results. Gueneau et al. [30] performed a single-crystal structure determination and chemical composition analysis. The recent work provided smaller lattice parameters based on the average model [30,31] for samples cast at 720 °C, indicating high Si content [63]. Krendelsberger et al. prepared a series AlFeSi alloys which were heat at heated at 550 °C for 1 month and 770 °C for two weeks. They observed τ_4 -phase in the samples with relatively high Si contents

(Table 3) and prepared at 550 °C [27]. There are small but systematic lattice parameter variations. The length of a -axis decreases with Si-content, which is consistent with our calculations (Fig. 3_top). Furthermore, they found no indications for a superlattice yielding an orthorhombic lattice. This is again because the preparation temperature is at 550 °C (823 K) is notably higher than the transformation temperature to the superstructure (660 K) and the average model is available, in agreement with our previous thermodynamics analysis. This is most likely the origin that most experimentalists using the average model for structural characterizations for this phase.

Here, the relative stability of the widely observed primary phases, θ -, cubic α - and hexagonal α' -, β -phase as well as the τ_4 -phase during casting of Al-alloys [9,29,65] is addressed. The definition of the formation energies is similar to Eqs. (1)–(3) with changes of the chemical compositions [5,38,52]. The relative stability of the binary and Si-containing ternary θ - and β -phases were investigated using the same code and settings as present work. The first-principles calculations for these phases are listed in Table 4.

Table 4 shows for the phases of highest stability, the contents of Si solution at the Al sites vary significantly. The highest Si content is for the τ_4 -Al₃Si₂Fe with 40.00 % Si in the total Al/Si sites. 18.2 % of the Al/Si sites were occupied by Si in β -phase, while there is only moderate Si content in θ -phase (5.1 %).

The relative stability of the binary θ -Al₁₃Fe₄, β -Al_{5,5}Fe and τ_4 -Al₅Fe phases has the order (from lowest formation energy to highest): θ - > β - >> τ_4 -phase. Meanwhile, for the ternary AlFeSi phases, the order is β - > θ - > τ_4 - phase with moderate energy differences (0.20 eV per Fe). These results mean strong impact on the formation of these phases. Clearly the high stability of the binary θ -Al₁₃Fe₄ phase indicates its dominance of formation in Si-poor Al alloys, while the relatively high Si containing β -Al_{4,5}SiFe phase form in the Al alloys of relative high Si contents. The relatively less stable τ_4 -(Al_{1-x}Si_x)₅Fe were experimentally observed less frequently and may form in high-Si Al alloys as shown in the experiments. This is also due to the high energy cost of Si solution in solid Al (0.43 eV/Si) (Table S-1), which forces the extra Si atoms to move into low potential regions, forming e.g. the τ_4 -phase particles in high-Si alloys. The energetics about the θ -, β -, τ_4 - phases help get some insight into the formation of the Fe-IMCs during casting. During casting, there is nucleation competition for these Fe-IMCs. Nucleation of one Fe-IMC phase requires precise structural and compositional templating and involves multiple alloying elements at specific atomic positions and necessitates substantial undercooling [66]. Unfortunately, the knowledge on the stability and structural properties for cubic α - and hexagonal α' -phases is still lacking, which hinders us to provide a complete picture, and this topic deserves further investigation.

5. Conclusions

First-principles density-functional theory calculations and thermodynamics analysis were utilized for investigating the intrinsic stability, chemical composition, interactions and structural and electronic properties of the τ_4 -(Al_{1-x}Si_x)₅Fe phase. This study justified the high stability of the τ_4 -Al₃Si₂Fe superstructure which is relatively stable at low temperature (< 430 K). Meanwhile the potential well on Si content is relatively shallow, which relates to compositional and structural flexibility of the τ_4 -phase. At temperature higher than 660 K, Si atoms are distributed at the Al/Si sites uniformly with the formula τ_4 -(Al_{1-x}Si_x)₅Fe, which is available for this phase in cast Al alloys. The Si content varies in τ_4 -(Al_{1-x}Si_x)₅Fe, depending on local chemical compositions. Moreover, the cell volume decreases linearly with increasing Si content.

The electronic structure calculations and chemistry analysis showed that τ_4 -(Al_{1-x}Si_x)₅Fe exhibits a triplet nature: metallic, ionic and covalent. Furthermore, there is a balance between electron count and repulsive Si-Si interaction in the crystal.

Table 4

The calculation results for the most stable binary AlFe and ternary AlFeSi compounds at 0 K, τ_4 -(this work), β -[38] and θ -[5,52] structures using the same code and settings.

Phase	Latt. S.G.	Latt.paras. (Å)	ΔE (eV/Fe*)	References and remarks
τ_4 -Al ₅ Fe	Tetra. <i>I4mcm</i> (nr.140)	$a = 6.262$ $c = 9.625$	- 0.64	This work [30,31] High Si solution at the Al sites.
τ_4 -Al ₃ Si ₂ Fe	Orth. <i>Pbcn</i> (nr.60)	$a = 6.059$ $c = 9.496$	- 1.08	Strong Si stabilization effect.
θ -Al ₁₃ Fe ₄	Monoclinic. <i>C2/m</i> (nr.12)	$a = 15.426$ $b = 8.022$ $c = 12.425$	- 1.13	Moderate Si solution at the Al ^{IX} sites according to the Grin's notation [64].
θ -Al _{12.33} Si _{0.67} Fe ₄	Monoclinic. <i>C2/m</i> (nr.12)	$a = 15.413$ $b = 8.015$ $c = 12.405$ $\beta = 107.68^\circ$	- 1.15	The Si stabilization effect is moderate.
β -Al _{5,5} Fe	Monoclinic. <i>A2/a</i> (nr. 15)	$a = 6.240$ $b = 6.240$ $c = 21.087$ $\beta = 90.34^\circ$	- 1.00	[38] Rather high Si solution and strong Si stabilization effect.
β -Al _{4,5} SiFe	Monoclinic. <i>A2/a</i> (nr. 15)	$a = 6.165$ $b = 6.165$ $c = 20.813$ $\beta = 91.43^\circ$	- 1.29	Si occupy the AlI or Al6 sites in the Romming's labels [65].

CRedit authorship contribution statement

changming Fang: Writing – review & editing, Writing – original draft, Visualization, Validation, Supervision, Software, Resources, Project administration, Methodology, Investigation, Funding acquisition, Formal analysis, Data curation, Conceptualization. **Zhongping Que:** Writing – review & editing, Supervision, Project administration. **Zhongyun Fan:** Writing – review & editing, Supervision, Project administration.

Declaration of Competing Interest

There is no interest conflict.

Acknowledgments

Dr. Qing Cai (BCAST) is acknowledged for benefit discussions. Financial support from the Engineering and Physical Sciences Research Council (EPSRC, UK) under Grand nos. EP/v011804/1 and EP/S005102/1 is gratefully acknowledged.

Appendix A. Supporting information

Supplementary data associated with this article can be found in the online version at doi:10.1016/j.jallcom.2025.182295.

References

- [1] W. Khalifa, F.H. Samuel, J.E. Gruzleski, Iron intermetallic phases in the Al corner of the Al-Si-Fe system, *Metal. Mater. Trans. A* 34 (2003) 807–825.
- [2] M.L. Glazoff, A. Khvan, V.S. Zolotarevsky, N.A. Belov, A. Dinsdale, Casting Aluminum Alloys: Their Physical and Mechanical Metallurgy, Butterworth-Heinemann, 2018.
- [3] V. Raghavan, Al-Fe-Si (aluminum-iron-silicon), *JPEDAV* 30 (2009) 184–188.
- [4] Z.P. Que, C.M. Fang, C.L. Mendis, Y. Wang, Z. Fan, Effects of Si solution in Al₁₃Fe₄ on phase transformation between Fe-containing intermetallic compounds in Al alloys, *J. Alloy. Compd.* 932 (2023) 167587.
- [5] C.M. Fang, Z.P. Que, A. Dinsdale, Z. Fan, Si solution in θ -Al₁₃Fe₄ from first-principles, *Intermetallics* 126 (2020) 106939.
- [6] L.A. Narayanan, F.H. Samuel, J.E. Gruzleski, Crystallization behavior of iron-containing intermetallic compounds in 319 aluminum alloy, *Metal. Mater. Trans. A* 25 (1994) 1761–1773.

- [7] V.A. Aranda, I.A. Figueroa, G. Gonzalez, J.A. García-Hinojosa, G.A. Lara-Rodríguez, Effect of small additions of Cr, Ti, and Mn on the microstructure and hardness of Al-Si-Fe-X alloys, *Metals* 9 (2019) 136.
- [8] Y. Li, B. Legendre, Enthalpy of formation of Al-Fe-Si alloys II (τ_6 , τ_2 , τ_3 , τ_8 , τ_4), *J. Alloy. Compd.* 302 (2000) 187–191.
- [9] Z.P. Que, Y. Wang, C.L. Mendis, C.M. Fang, J.H. Xia, X.R. Zhou, Z. Fan, Understanding Fe-containing intermetallic compounds in Al alloys: an overview of recent advances from the LiME research hub, *Metals* 12 (2022) 1677.
- [10] M. Warmuzek, Chemical composition of the Ni-containing intermetallic phases in the multicomponent Al alloys, *J. Alloy. Compd.* 604 (2014) 245–252.
- [11] Q. Cai, C.M. Fang, E. Lordan, Y. Wang, I.T.H. Chang, B. Cantor, A novel Al-Si-Ni-Fe near-eutectic alloy for applications at elevated temperatures, *Scr. Mater.* 237 (2023) 115707.
- [12] L.F. Zhang, J.W. Gao, L. Nana, W. Damoah, D.G. Robertson, Removal of iron aluminum: a review, *Miner. Process. Extr. Metall. Rev.* 33 (2012) 99–157.
- [13] M.E. Schlesinger, Aluminum Recycling, CRC Press, Boca Raton, 2006.
- [14] M.A. Reuter, A. van Schaik, J. Gutzmer, N. Bartie, A. Abadías-Liomas, Challenges of the circular economy: a material, Metallurgical, and Product design perspective, *Ann. Rev. Mater. Res.* 49 (2019) 253–274.
- [15] H.R. Kotadia, N. Bareker, M.H. Khan, J.L. Ahuir-Torres, A. Das, Aluminium recycling: a critical review of iron-bearing intermetallics in alloys, *Mater. Today Sustain.* 30 (2025) 101119.
- [16] W. Mohammed, X.R. Chen, D. Ponge, D. Raabe, Thermodynamics-guided design of sustainable secondary Al-Si alloys for enhanced Fe-impurity tolerance and optimized Mn doping, *Acta Mater.* 289 (2025) 120932.
- [17] H.B. Chen, Y.L. Xie, P. Tang, Z.Y. Tang, C.W. Liao, R.H. Pang, Demystifying the influence of scrap to raw material ratio on the microstructural and mechanical properties of the secondary 7075 aluminum alloy, *Mater. Lett.* 382 (2025) 137847.
- [18] G. Gaustad, E. Olivetti, R. Kirchain, Improving aluminum recycling: a survey of sorting and impurity removal technologies, *Resour. Conserv. Recycl.* 58 (2012) 79–87.
- [19] N. Krendelsberger, F. Weitzer, J.C. Schuster, On the reaction scheme and liquidus surface in the ternary system Al-Fe-Si, *Metal. Mater. Trans. A* 38 (2007) 1681–1691.
- [20] P.V. Liddicoat, X.-Z. Liao, Y.H. Zhao, Y.T. Zhu, M.Y. Murashkin, E.J. Lavernia, R. Z. Valiev, S.P. Ringer, Nanostructural hierarchy increases the strength of aluminium alloys, *Nat. Commun.* 1 (2010) 63.
- [21] L.M. Qin, P. Tang, S.X. Meng, Effect of Ni addition on the microstructure, conductivities and mechanical properties of as-cast Al-Fe alloys, *J. Alloy. Compd.* 986 (2024) 174160.
- [22] V. Raghavan, Al-Fe-Si (aluminum-iron-silicon), *JPEDAV* 32 (2011) 140–142.
- [23] G. Ghosh, Aluminium-iron-silicon, in: G. Effenberg, S. Llyenko (Eds.), *Landolt-Börnstein – Group IV Physical Chemistry 11D1 (Iron Systems, Part 1)*, Landolt-Börnstein, Stuttgart, 2008.
- [24] M.V. Kral, P.N.H. Nakkashima, D.R.G. Mitchell, Electron microscope studies of Al-Fe-Si intermetallics in an Al-11 pct Si alloy, *Metal. Mater. Trans. A* 37 (2006) 215–219.
- [25] H. Becker, T. Bergh, P.E. Vullum, A. Leineweber, Y. Li, beta- and delta-Al-Fe-Si intermetallic phase, their intergrowth and polytype formation, *J. Alloy. Compd.* 780 (2019) 917–929.
- [26] H.P. Takeda, K. Mutuzaki, The equilibrium diagram of the iron-aluminium-silicon system, *Tetsu to Hagane* 26 (1940) 335–361 (in Japanese).
- [27] O.S. Zarechnyuk, N.V. German, T.I. Yanson, R.M. Rykhal, A.A. Murav'eva, Some phase diagrams of aluminium with transition metals, rare earth metals and silicon. *Fazovje Ravnesovija v metalicheskych splavach (in Russian)*, Nauka, Moscow, 1981, pp. 69–71.
- [28] M.V. Kral, A crystallographic identification of intermetallic phases in Al-Si alloys, *Mater. Lett.* 59 (2004) 2271–2276.
- [29] C.J. Todaro, M.A. Easton, D. Qiu, G. Wang, D.H. StJohn, M. Qian, Effect of ultrasonic melt treatment on intermetallic phase formation in a manganese-modified Al-17Si-2Fe alloy, *J. Mater. Proc. Technol.* 271 (2019) 346–356.
- [30] C. Gueneau, C. Servant, F. D'Yvoir, N. Rodier, FeAl_3Si_2 , *Acta Crystallogr. C* 51 (1995) 177–179.
- [31] P.K. Pandey, K. Schubert, Strukturuntersuchungen in einigen mischungen T-B3-B4 (T = Mn, Fe, Co, Ir, Ni, Pd; B3 = Al, Ga, Tl; B4 = Si, Ge), *J. Less-Common Met.* 18 (1969) 175–202.
- [32] T. Sasaki, T. Kato, J. Fukushima, Y. Hayashi, H. Takizawa, High-pressure synthesis and crystal structure of a novel intermetallic compound $\text{Mn}(\text{Al}, \text{Ge})_5$, *J. Alloy. Compd.* 806 (2019) 58–62.
- [33] J.E. Tibballs, R.L. Davis, B.A. Parker, Al-Si substitution in α -phase AlMnSi , *J. Mater. Sci.* 24 (1989) 2177–2182.
- [34] M. Cooper, K. Robinson, The crystal structure of the ternary alloy $\alpha(\text{AlMnSi})$, *Acta Cryst.* 20 (1966) 614–617.
- [35] P. Donnadiou, G. Lapasset, T.H. Sanders, Manganese-induced ordering in the α -(Al-Mn-Fe-Si) approximant phase, *Philos. Mag. Lett.* 70 (1994) 319–326.
- [36] J. Wang, S.L. Shang, Y. Wang, Z.G. Mei, Y.F. Liang, Y. Du, Z.K. Liu, First-principles calculations of binary compounds: Enthalpies of formation and elastic properties, *CALPHAD* 35 (2011) 562–573.
- [37] S.L. Shang, J. Wang, Y. Wang, Y. DU, Z.K. Liu, Phonon and thermodynamic properties of Al-Mn compounds: a first-principles study, *Comput. Mater. Sci.* 50 (2011) 2096–2103.
- [38] C.M. Fang, Z.P. Que, Z. Fan, Crystal chemistry and electronic structure of the β -AlFeSi phase from first-principles, *J. Solid State Chem.* 299 (2021) 122199.
- [39] L. Amirkhanyan, T. Weissbach, T. Gruber, T. Zienert, O. Fabricnaya, J. Kortus, Thermodynamic investigation of the Ta4-Al-Fe-Si intermetallic ternary phase: a density-functional theory study, *J. Alloy. Compd.* 298 (2014) 137–141.
- [40] Z.F. Hou, Y. Takagiwa, Y. Shinohara, Y.B. Xu, K. Tsuda, First-principles study of electronic structures and elasticity of $\text{Al}_2\text{Fe}_3\text{Si}_3$, *J. Phys. Condens. Matter* 33 (2021) 195501.
- [41] D. Raabe, D. Ponge, P. Uggowitzer, M. Roscher, M. Paolantonio, C. Liu, H. Antrekowitsch, E. Kozeschnik, D. Seidmann, B. Gault, et al., Making sustainable aluminium by recycling scrap: the science of “dirty” alloys, *Prog. Mater. Sci.* 128 (2022) 100947.
- [42] Q.F. Jiang, P. Tang, H. Jiang, Synergistic effect of in-situ TiC particles synthesis on microstructure and mechanical properties of Fe-rich eutectic Al-Si alloy, *Mater. Today* 41 (2024) 110257.
- [43] G. Kresse, J. Hafner, *Ab initio* molecular-dynamics simulation of the liquid-metal-amorphous-semiconductor transition in germanium, *Phys. Rev. B* 49 (1994) 14251–14269.
- [44] G. Kresse, J. Furthmüller, Efficiency of *ab-initio* total energy calculations for metals and semiconductors using a plane-wave basis set, *Comput. Mater. Sci.* 6 (1996) 15–50.
- [45] P. Hohenberg, W. Kohn, Inhomogeneous electron gas, *Phys. Rev.* 136 (1964) B864–B871.
- [46] P.E. Blöchl, Projector augmented-wave method, *Phys. Rev. B* 50 (1994) 17953–17978.
- [47] J.P. Perdew, K. Burke, M. Ernzerhof, Generalized gradient approximation made simple, *Phys. Rev. Lett.* 77 (1996) 3865–3868.
- [48] C.M. Fang, M.A. van Huis, M.H.F. Sluiter, H.W. Zandbergen, Stability, structure and electronic properties of $\gamma\text{-Fe}_{23}\text{C}_6$ from first-principles theory, *Acta Mater.* 58 (2010) 2968.
- [49] H.J. Monkhorst, J.D. Pack, Special points for Brillouin-zone integrations, *Phys. Rev. B* 13 (1976) 5188–5192.
- [50] J. Arblaster, Selected Values of the Crystallographic Properties of the Elements, ASM International, Materials Park, Ohio, 2018.
- [51] W. Pepperhoff, M. Acet, The magnetism of iron, in: *Constitution and Magnetism of Iron and its Alloys*. Engineering Materials, Springer, Berlin, Heidelberg, 2001.
- [52] C.M. Fang, A. Dinsdale, Z.P. Que, Z. Fan, Intrinsic defects in and electronic properties of $\theta\text{-Al}_3\text{Fe}_4$: an *ab initio* DFT study, *J. Phys. Mater.* 2 (2019) 015004.
- [53] A. Dinsdale, C.M. Fang, Z.P. Que, Z. Fan, Understanding the thermodynamics and crystal structure of complex Fe containing intermetallic phases formed on solidification of aluminium alloys, *JOM* (2019) 1731–1736.
- [54] R.F.W.A. Bader, A quantum theory of molecular structure and its applications, *Chem. Rev.* 91 (1991) 893–928.
- [55] R.F.W. Bader, A bond path: a universe indicator of bonded interactions, *J. Phys. Chem. A* 102 (1998) 7314–7323.
- [56] G. Henkelman, A. Arnaldsson, H. Jonsson, A fast and robust algorithm for Bader decomposition of charge density, *Comput. Mater. Sci.* 36 (2006) 254–360.
- [57] L. Pauling, The nature of the chemical bond. IV. The energy of single bonds and the relative electronegativity of atoms, *J. Am. Chem. Soc.* 54 (1932) 3570–3582.
- [58] E.C. Stoner, Collective electron ferromagnetism, *Proc. R. Soc. A* 165A (1938) 372–414.
- [59] C.M. Fang, Z.P. Que, Z. Fan, Effects of Si solution on stability of early 3d transition-metal tri-aluminides, Al_3T (T = Sc, Ti and V), *JOM* 77 (2025) 1091–1102.
- [60] M. Zedalis, M.E. Fine, Lattice parameter variation of $\text{Al}_3(\text{Ti}, \text{V}, \text{Zr}, \text{Hf})$ in Al-2 at% (Ti, V, Zr, Hf) alloys, *Scr. Met.* 17 (1983) 1247–1251.
- [61] J.-R. Castillo-Sánchez, G. Salloum-Abou-Jaoude, A.E. Gheribi, P. Lafaye, K. Oishi, J.-P. Masse, E. Bousser, G. L'Espérance, J.-P. Harvey, Synthesis and characterization of $(\text{Al}, \text{Si})_3(\text{Zr}, \text{Ti})\text{-D}_{022}/\text{D}_{023}$ intermetallics: understanding the stability of silicon substitution, *Acta Mater.* 262 (2023) 119455.
- [62] V.J. Yannello, D.C. Fredrickson, Generality of the 18-n rule: intermetallic structural chemistry explained through isolobal analogies to transition metal complexes, *Inorg. Chem.* 54 (2015) 11385–11398.
- [63] Z.P. Que, unpublished results.
- [64] Y. Grin, U. Burkhard, M. Ellner, K. Peters, Refinement of the Al_3Fe_4 structure and its relationship to the quasihomological homeotypical structures, *Z. Krist.* 209 (1994) 479–487.
- [65] C. Rømming, V. Hansen, J. Gjønnes, Crystal structure of $\beta\text{-AlFeSi}$, *Acta Crystallogr. B* 50 (1994) 307–312.
- [66] Z.P. Que, C.M. Fang, Z. Fan, Nucleation competition and phase transformation mechanisms in recycled aluminium alloys: insights into $\theta\text{-Al}_3\text{Fe}_4$, $\text{Al}_6(\text{Fe}, \text{Mn})$ and $\alpha\text{-Al}_{15}(\text{Fe}, \text{Mn})_3\text{Si}_2$, *J. Alloy. Compd.* (2025) 181130.